Proceedings of the 7th International Conference on the Application of Physical Modelling in Coastal and Port Engineering and Science (Coastlab18)
Santander, Spain, May 22-26, 2018

INTERSTITIAL FLOW FIELD MEASUREMENTS OF A MONOCHROMATIC WAVE IN A TWO-DIMENSIONAL, RECTANGULAR, NON-STAGGERED POROUS STRUCTURE

LUTHER TERBLANCHE[1], GERHARDUS DIEDERICKS[2], FRANCOIS SMIT[3], CHRISTOPHE TROCH[4]

1 Stellenbosch University, South Africa, Luther.Terblanche@gmail.com
2 Stellenbosch University, South Africa, hardus@sun.ac.za
3 Stellenbosch University, South Africa, fsmit@sun.ac.za
4 Council for Scientific and Industrial Research, South Africa, ctroch@csir.co.za

ABSTRACT

In this study the velocity field measurement of monochromatic waves traversing an idealised porous medium was conducted. A two-dimensional, rectangular porous structure was built from timber beams and arranged in a non-staggered array. The structure was placed inside a glass wave flume where the interaction of a monochromatic wave with the porous structure was observed. The portion of the array that was below the waterline, were divided into overlapping regions, each of which were carefully seeded in a sequential manner with neutrally buoyant microspheres. The region being measured was illuminated with an LED light source and filmed with a high speed video camera. The water levels inside the porous structure were simultaneously measured with capacitance probes. The recorded images from the high speed camera, were processed and analysed with image processing and PIV techniques to derive a velocity field for one wave cycle at each region. The velocity fields at all the regions were combined to obtain the best estimate of the flow field through the entire porous structure for one wave cycle.

KEYWORDS: Waves, Porous Media, PIV, Velocity Measurements.

1 INTRODUCTION

Porous structures are widely used as breakwaters in ports to provide shelter for moored vessels against ocean swell waves. Many beach nourishment schemes also depend on porous structures in the form of groins. Hence, the interaction of waves with porous structures has been a topic of significant interest over the past number of decades.

Different facets of the interaction between waves and porous structures have been studied by different researchers over the years. These include classical theoretical models used to obtain expressions for the reflection and transmission coefficients of waves interacting with different types of porous structures (Sollitt and Cross, 1976; Madsen, 1974; Madsen, 1983). In recent years with the aid of computer processing power, more sophisticated models could be solved numerically to determine the effects of porous structures on waves, such as non-hydrostatic models (Ma, 2014) and fully integrated Volume of Fluid models (Higuera *et al.*, 2014).

Several experimental studies on wave interaction with porous structures have also been published. The type of structures experimentally tested varied from rubble mound rectangular and triangular structures (Mellink, 2012) to lattice type ideal structures (Kondo and Toma, 1972, Losada *et al.*, 1995).

Wave induced interstitial flow velocity measurements inside porous media are limited. Comprehensive velocity measurements over the complete porous domain would give valuable physical insight into the processes that influence wave transmission and reflection inside a porous medium. Losada *et al.*, 1995, performed velocity measurements in a lattice type structure, but only at selected discrete positions. This work is an attempt to provide a more complete velocity field measurement of monochromatic waves traversing an idealised porous medium.

2 EXPERIMENTAL SET-UP

The experimental work was carried out at the Coastal and Hydraulics Laboratory of the Council for Scientific and Industrial research (CSIR) in Stellenbosch, South Africa. The laboratory is an 11 000 m^2 facility with infrastructure to accommodate both 2D and 3D physical model studies.

2.1 Flume

A glass flume, which is 1 m deep, 33 m long and 0.75 m wide, was used for the research work. The flume is fitted with an HR Wallingford piston type shallow water wave generator which has active wave absorption capability to compensate for reflected waves at the wave maker paddle. A photograph of the flume and a sketch of the experimental set-up is shown in Figure 1.

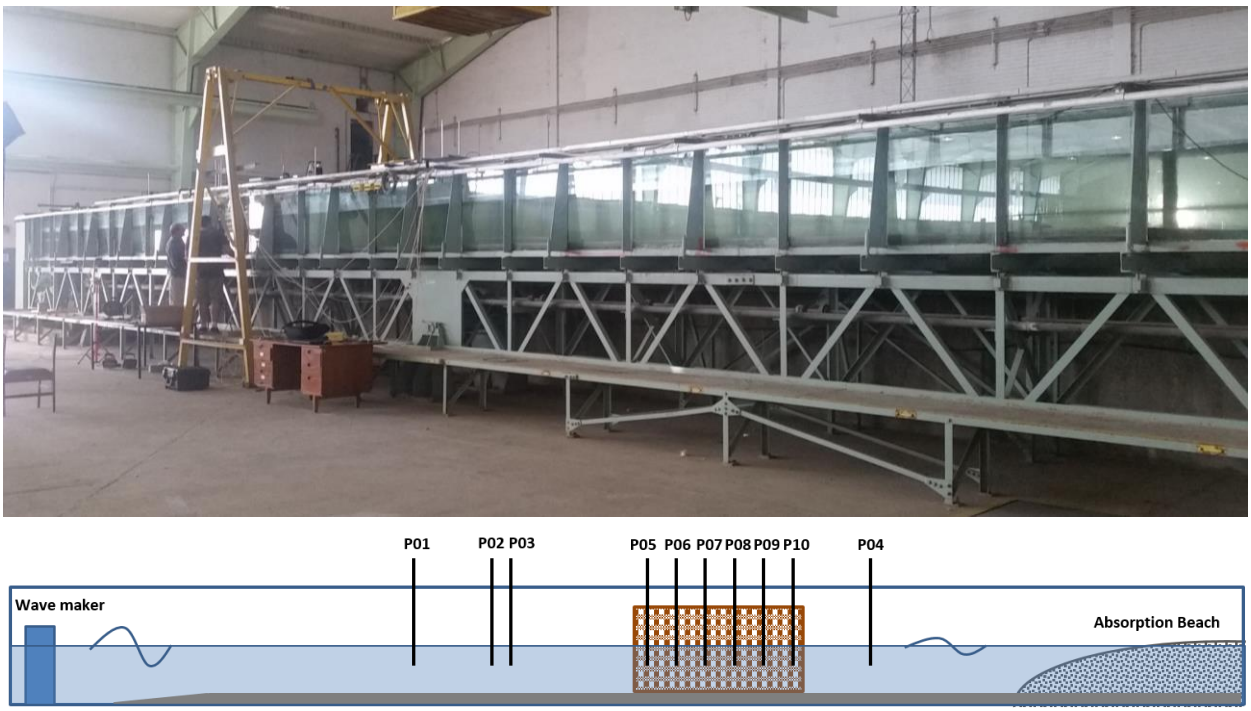

Figure 1: Glass flume at the CSIR Coastal and Hydraulics Laboratory.

2.2 Structure

An ideal two-dimensional porous medium was constructed from 171 rectangular timber beams, arranged in an array of 9 equally spaced rows and 19 equally spaced columns. The beams, with nominal dimensions 0.04 m x 0.04 m x 0.73 m, were sourced from a local wood factory. Slight variations on the dimensions of the beams were unavoidable, but minimal.

The two-dimensional porous medium was assembled in tree parts, which were then lifted into the flume. The three parts were constructed by drilling an array of holes, 0.08 m apart, into 6 acrylic panes. The beams were fitted with dowels on either end and fitted to the acrylic panes to form the parts of the porous medium. A photograph of the porous medium, fitted into the glass flume, is shown in Figure 2.

The yellow labels, D01-D70 indicate the pores where velocity measurements were taken and the red labels, P05-P10, indicate the positions where capacitance probes were fitted to measure the water surface elevation inside the porous medium.

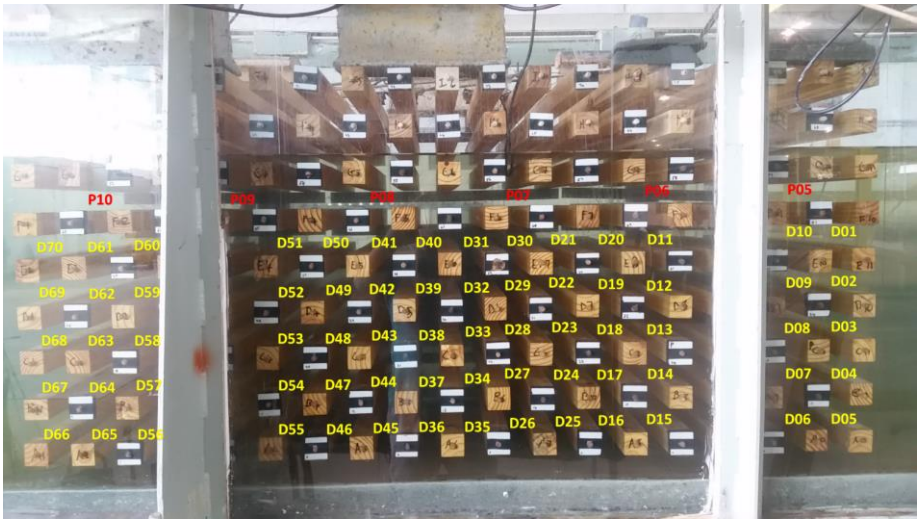

Figure 2: Ideal two-dimensional porous medium fitted in the glass flume.

2.3 Measurement Equipment

2.3.1 Water Surface Elevations

The water surface elevations were measured with 10 capacitance probes (Figure 3), sampling at a rate of 50 Hz. Three probes were placed on the wave maker side of the structure and one probe on the lee side. The distance between

the first and the second probe (P01 and P02) was 0.390 m and the distance between the second and third probe (P02 and P03) was 0.069 m. These three probes were used to obtain estimates of the incident and reflected wave heights with the three probe method of Mansard and Funke, 1980. The probe on the lee side of the structure was used to estimate the wave transmission through the structure.

Six capacitance probes were fitted inside the porous medium, 0.240 m apart. The positions of the internal capacitance probes (P05 – P10) are shown in red in Figure 2. Due to the space constraint inside the porous medium, the capacitance wires were fixed directly to the wooden beams with pins. The internal capacitance probes were therefore immovable and had to be calibrated by rising and lowering the water level. The external capacitance probes were fitted to adjustable probe stands which could be lowered and raised for calibration.

Figure 3: Capacitance probe on a probe stand.

2.3.2 Flow Field

Fluorescent green polyethylene microspheres with a density of 1000 kg/m^3 and a diameter of 300-355 µm were acquired from *Cospheric* and used for the visualization of the flow field. The particles are near neutrally buoyant in fresh water and therefore capable of following the flow field accurately. The size of the beads were chosen large enough to be clearly visible to the naked eye, but also small enough to not influence the flow field inside the pores. Care was also taken to ensure that the diameter of the beads on the digital image captured by the camera were ~2 pixels, which is the optimal recommended size for particle image velocimetry (PIV) (Raffel *et al.*, 2007).

In most PIV applications a Charge-Coupled Device (CCD) camera is linked to a pulsating sheet laser via a synchronizer which determines exactly when the flow field is illuminated and an image taken. The main benefit of using a sheet laser is that only the particles in the plane section of interest are illuminated for a very short period of time and the measurements are not affected by 3D features in the flow field. Such a measurement system is fairly expensive and it is not practically to set up a laser sheet in a porous structure such as the one being tested.

The flow field in the experimental setup was predominantly two-dimensional with minimal velocity components over the width of the flume. This meant that the beads, after seeding, would more or less stay in one plane section. A high speed camera (Olympus i-Speed TR3) was fitted with a Nikkor 17-55 mm f/2.8G lens at a focal length of 55 mm to keep perspective distortion to a minimum. The lens was set to have a shallow depth of field (e.g., f-stop value of f/8.0 to f/11.0). The beads that fall inside the depth of field would appear sharp edged while the ones outside the depth of field would be blurred or not visible at all. The camera was set-up to take 100 frames per second at a resolution of 1280 by 1024 pixels. A photograph of the high speed camera and the light source on tripods in front of the structure in the flume is shown in Figure 4.

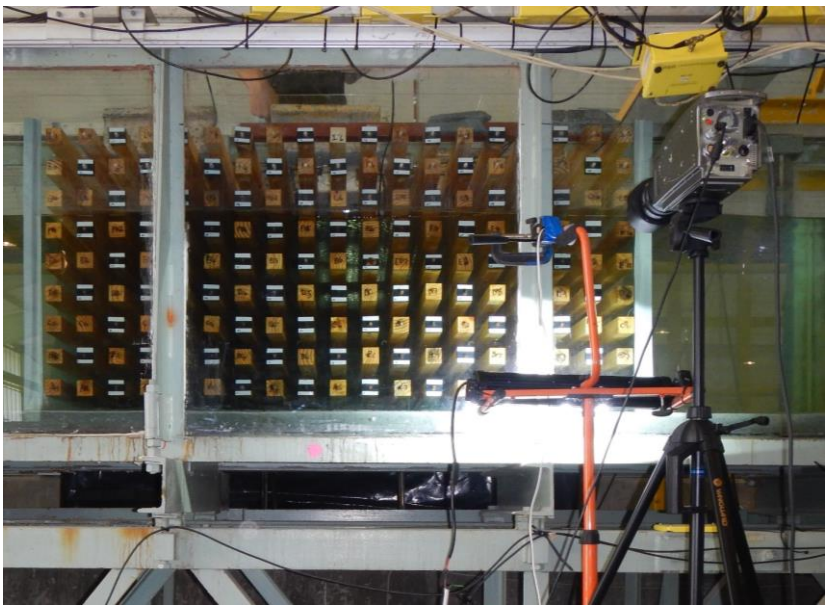

Figure 4: Image of the experimental set-up showing the high speed camera and light source.

The light source consisted of a series of twelve 10 Watt Cree XP-L HI LEDs that emit a stable white light so that each frame captured by the high speed camera has the same level of exposure. The light source was supplemented by individual 50 W LED lights that was directed at the pore of interest to illuminate any shadow zones from the main light source.

2.4 Test conditions and description

The water depth at the structure was set at 0.5 m. A monochromatic wave with an incident wave height of 0.032 m and a period of 1 second was tested.

The waves were generated by an HR Wallingford piston type shallow water wave generator with active wave absorption to minimize re-reflection of waves into the domain. The incident waves are partially reflected at the structure, and the amount of reflection is measured by the three probes in front of the structure (P01 – P03 in Figure 1).

The waves that enter the structure attenuate and are transmitted through the lee side of the structure. The amount by which the waves is attenuated is measured by six probes (P05 – P10 in Figure 1) inside the structure, and the transmitted wave heights are measured by the probe at the back of the structure (P04 in Figure 1).

The transmitted waves dissipates on a concave gravel absorption beach at the back of the structure. The reflection coefficient from the absorption beach was measured by running waves in the flume without the structure. For the particular wave conditions tested, the reflection coefficient of the absorption beach were determined to be about 5%.

3 MEASUREMENTS

3.1 Water Level Measurements

The water surface elevations were measured with capacitance probes, as described in section 2.3.1, at 6 locations inside the porous medium. The water elevation measurements contained some high frequency noise, which was removed with a low pass frequency filter. The raw time series of five wave cycles of probe 7 as well as the associated filtered signal is shown on the left hand side of Figure 5.

Zero crossing analyses were performed on the water surface elevations and the mean wave height was determined from the zero crossing analyses and is plotted in the graph on the right hand side of Figure 5. An exponential decrease of wave height inside the porous structure is visible.

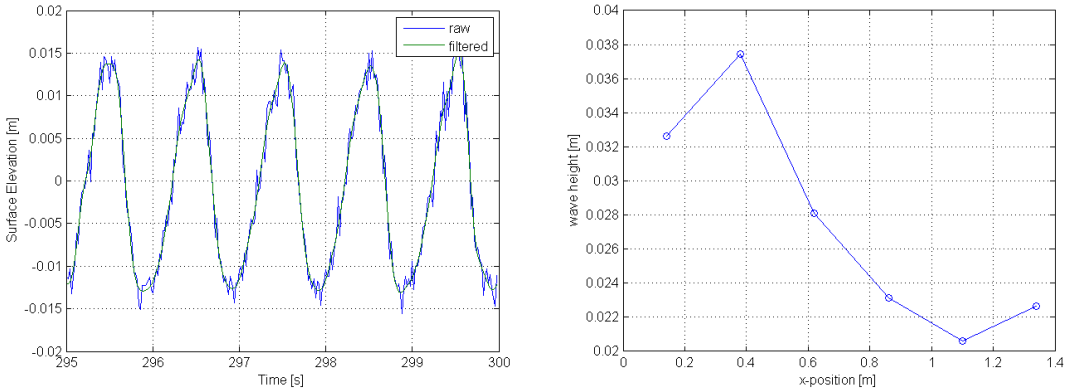

Figure 5: Raw and filtered surface elevation of probe 7 (left) and wave heights inside the porous structure (right).

3.2 Velocity Measurements

The polyethylene microspheres were sourced from Cospheric and came in powder form. Polyethylene is hydrophobic and the beads had to be coated with a surfactant prior to suspension in water. Wynns Gleen Green was used as the surfactant to lower the water tensions. A syringe connected to a tube fastened to a steel rod was used to draw up a portion of the bead solution to seed the fluid in the specific pore that was being recorded by the high speed camera.

The seeding was done by inserting the tubing in between the openings of the structure. The end of the tubing was then positioned in the lower region of the pore that was being recorded. The bead solution was then slowly released through the opening at the end of the tubing while slowly lifting the tubing upwards for an even distribution of beads across the pore. Guide rails were placed at the entry point at the top of the structure to guide the steel rod into position and to keep a constant distance from the side of the flume (and the camera lens). A typical seeding process is illustrated in Figure 6 in 4 time frames.

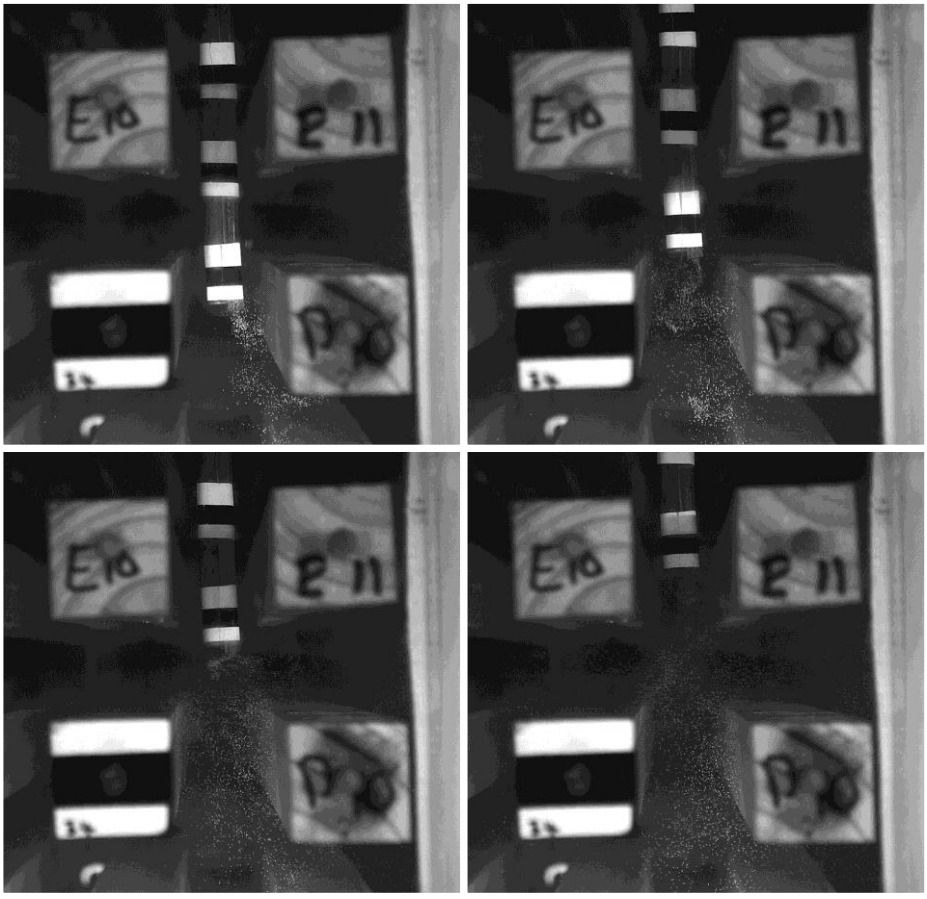

Figure 6: The seeding of a pore at 4 different time frames (read left to right, top to bottom).

After each seeding, approximately 15 wave cycles were recorded with the high speed camera. All 70 pores shown in Figure 2 were recorded in the numeric order they are labelled in Figure 2. The pores near the water surface were the most challenging to measure. Near the water surface the velocities are the highest and the free surface interacts with the beams. This causes some level of turbulence and introduce three-dimensional velocity effects which cause the beads to disperse rather quickly and some go out of focus.

Another area that was challenging to measure was the pores near the bed where the orbital velocities are relatively small. To obtain an even distribution of beads in the bottom pores, the end of the tubing had to be moved around carefully during the seeding process. This action created small eddies that disturbed the flow field to some extent and these effects required time to fully dissipate. A net return velocity was also observed in the near-bed layer which transported the beads in the direction of the incoming waves with each wave cycle.

4 ANALYSES

Particle image velocimetry analyses of the high speed video images were conducted with the open source tool PIV-Lab (Thielicke and Stamhuis, 2014). The software PIV-Lab has several built in algorithms for image pre-conditioning, sub-pixel peak estimators, data validation and interpolation and smoothing. The user can run PIV-Lab from a GUI or from the MATLAB command line interpreter with user defined scripts and functions.

4.1 Image pre-processing

Each of the recorded images where cropped to the area of interest and converted to 8-bit gray scale for increased processing speed. The following image processing techniques where applied to the images to enhance the quality for image correlation:

1. Histogram equalization – A contrast limited adaptive histogram equalization (CLAHE) algorithm was applied to the images to improve the local contrast without over amplifying noise;
2. Intensity high-pass filter – A high-pass filter was applied to the images to suppress low frequency background information and emphasise the particles. A filter size of 5 pixels was used.
3. Intensity capping – Additional intensity capping was included where the intensity of very bright spots was limited to reduce statistical bias in the correlation signal.
4. Wiener noise filter – An adaptive low-pass Weiner filter was used to filter noise from each image.

An example of an original and pre-processed image is shown in Figure 7.

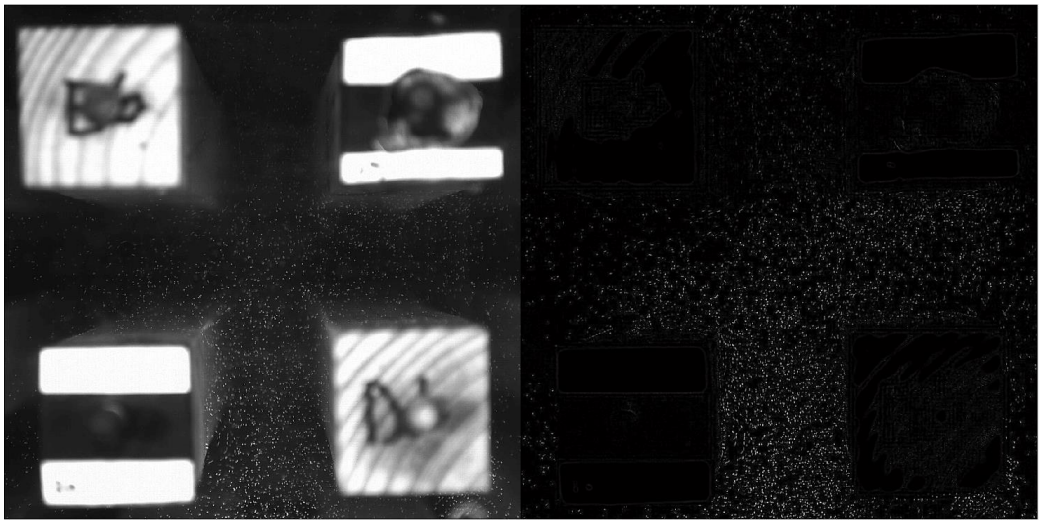

Figure 7: Original cropped 8-bit grayscale image (left) and pre-processed image (right)

4.2 Particle image velocimetry analysis

Standard cross correlation techniques were used in the PIV analysis. Two consecutive images in time (say A and B) were divided into smaller, overlapping, sub-images, referred to as interrogation areas. These interrogation areas were cross correlated in the frequency domain by applying a Fast Fourier Transform (FFT). Two passes of cross correlation were carried out. In the first pass the interrogation areas were 64x64 pixels with a step size of 32 pixels.

In the second pass, information from the first cross correlation analysis was used to offset and deform the interrogation areas in the second cross correlation calculation. This insures higher accuracy at a finer spatial resolution. The interrogation areas and step size of the seconds cross correlation were 40x40 pixels and 20 pixels, respectively. The

deformation of the interrogation windows in the second pass was determined by the velocities at the corner points of the interrogation areas. Velocities in regions with sheer flows can be calculated with higher precision with the use of a multi-pass system that accounts for the interrogation area deformation.

A two-dimensional Gaussian function was fitted to the nine discrete points surrounding the intensity peak in the cross correlation matrix. The position of the maximum of the 2D Gaussian function was then determined to obtain a sub-pixel estimate of the displacement of the interrogation window between the two consecutive images in time. These pixel displacements at the discrete steps of the interrogation windows, together with the frame rate of the images, form the velocity vector field in pixels/frame.

4.3 Post-processing

One of the most important aspects of post processing PIV results is the validation of the vector data obtained from the analysis. Several factors may influence the quality of the cross correlation matrix, such as the quality of the image, or the amount of particles at a given location in the image, etc. This may lead to spurious velocity vectors that deviate unphysically in magnitude and/or direction from nearby valid vectors.

A common and simple method to detect outlier vectors is to set upper and lower thresholds, characterized by a user defined multiple of standard deviations from the mean of velocity components. Another more sophisticated method that automatically accounts for local flow patterns that may substantially differ from the main flow field is the normalized median test (Westerweel and Scarano, 2005). The normalized median uses the 3 x 3 neighborhood data of a displacement vector to calculate a residual by subtracting the median of the 8 neighboring displacement vectors. These residuals are then normalized by the median of the residuals of the neighboring displacement vectors as follows

$$r' = \frac{|U_i - U_m|}{\varepsilon \cdot r_m}, \tag{1}$$

where $U_i, i = 1 \dots 8$ are the neighboring displacement vectors of U_0, $U_m$is the median of $U_i, i = 1 \dots 8$. r_m, is the median of $r_i, i = 1 \dots 8$ where $r_i = |U_0 - U_i|, i = 1 \dots 8$, and ε is an arbitrary small constant that avoids the enumerator from striving towards zero in near uniform flow regions.

The residual calculated with equation (1) can be used to reject spurious outlier vectors in a complex flow field that includes laminar and turbulent flow regions with a single threshold parameter. A threshold value of 2 was shown to be an appropriate choice for many different benchmark cases in literature (Westerweel and Scarano, 2005). Smaller and larger values for the threshold would lead to a more stringent or less stringent outlier detection, respectively.

After spurious vectors are removed with outlier detection methods, the gaps are usually filled with some form of interpolation. An interpolation method used by PIV-Lab is based on a boundary value solver (D'Errico, 2012). In this method the missing data (or holes) on a regular grid are estimated by solving a partial differential equation (PDE) that is assumed to represent the missing features. The values on the edges of the missing portion of data are used as boundary values to the PDE. A few types of PDEs can be used in this method, of which the Laplace equation is the default.

4.4 Data synthesis

Velocity fields were measured separately for each of the 70 pores. The velocity fields of the individual pores were merged to form a single velocity field that represents the entire measured pore space. Two main challenges are associated with the data fusion:

1. Since each pore was measured independently from all of the other pores, the time synchronization between the pores was lost. Each of the pore velocity measurements had to be matched in time to form a continuous flow field from one pore to the next.
2. Not all areas of each of the pores were filled with beads during the measurements. Hence there are gaps in the measured velocity fields of the pores. In certain cases these gaps could be filled with velocity measurements from a neighboring pore.

The time synchronization of the pore velocity field measurements were achieved by two steps:

1. Synchronizing each column of pores.
2. Synchronizing all columns with each other.

Each column of pores where synchronized by calculating the average pore velocity for each pore per time step. The velocity field of each pore was then time shifted such that the vertical velocity component of the average pore velocity is at a maximum at zero time.

Next, each column was synchronized as a whole by assigning a time lag to the velocity field, relative to the first column. The time lag of each column was calculated from the phase speed of the transmitted wave inside the porous medium. The phase speed of the transmitted wave was determined by applying a cross correlation function on adjacent internal probes to estimate the time lag between the two signals. The distances between the probes are known and hence the phase speed of the transmitted wave can be determined.

The filtered measured surface elevations of probe 6 and probe 7 are shown on the left hand side of Figure 8, showing the time lag water surface elevation. The celerity of the transmitted wave at the various internal probe locations is shown on the right hand side of Figure 8. Some variation in the celerity was observed, which may be attributed to internal wave reflections. The mean transmitted wave celerity is approximately 1.013 m/s and is indicated by the black dashed line.

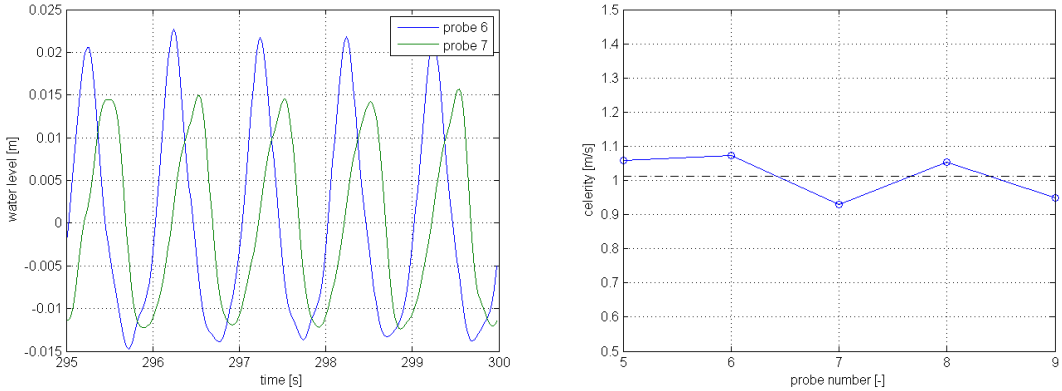

Figure 8: Filtered water surface elevation measurement of probes 6 and 7 (left), calculated transmitted wave celerity at probes 6 to 9 (right)

Figure 9 shows the merged spatial distribution of the velocity magnitude for an instant in time (t = 0.4 s). The top figure is the merged synchronized measurements where the outlier vectors were removed. The bottom figure is after the missing data has been interpolated onto a regular grid with a spacing of 0.002 m. The two columns of missing data are where the metal frame of the flume obscured the camera view.

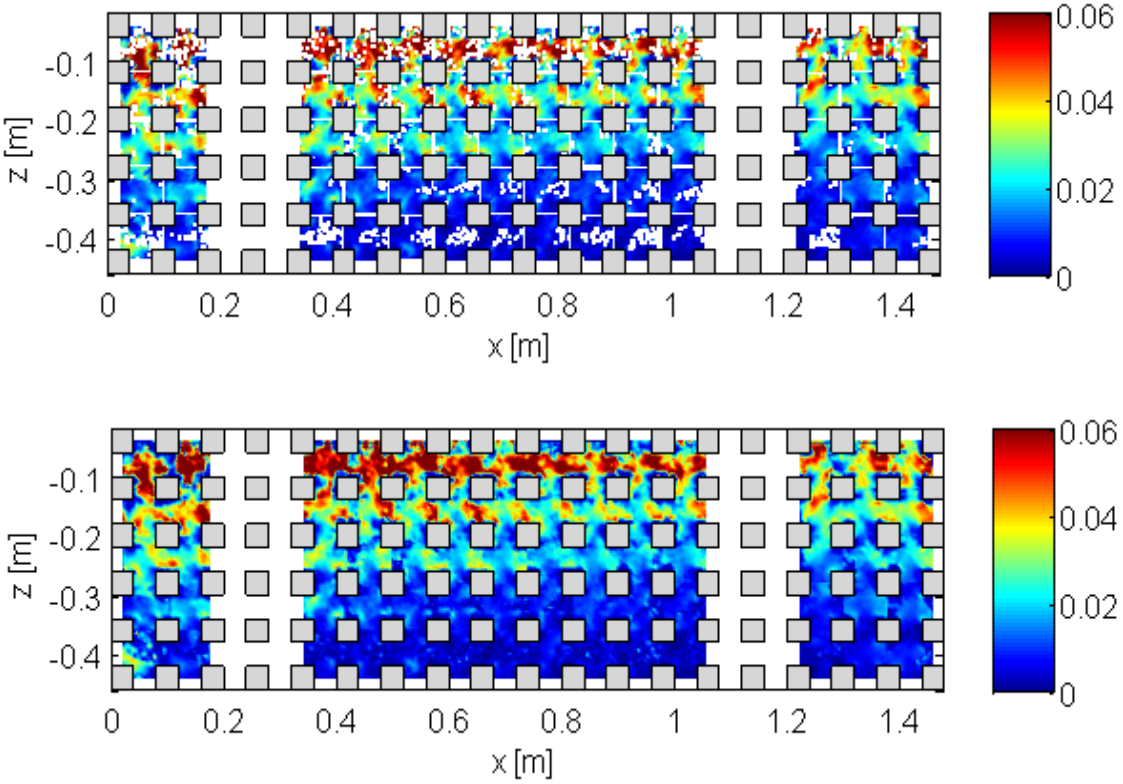

Figure 9: Merged and synchronised velocity magnitude (top), and interpolated (bottom).

Figure 10 shows the interpolated measured velocity field of 6 pores. The velocity vector field is fairly smooth across pores. This indicates that synchronization and calibration of each pore were effective, and that the measured data was successfully merged to form a continuous velocity field.

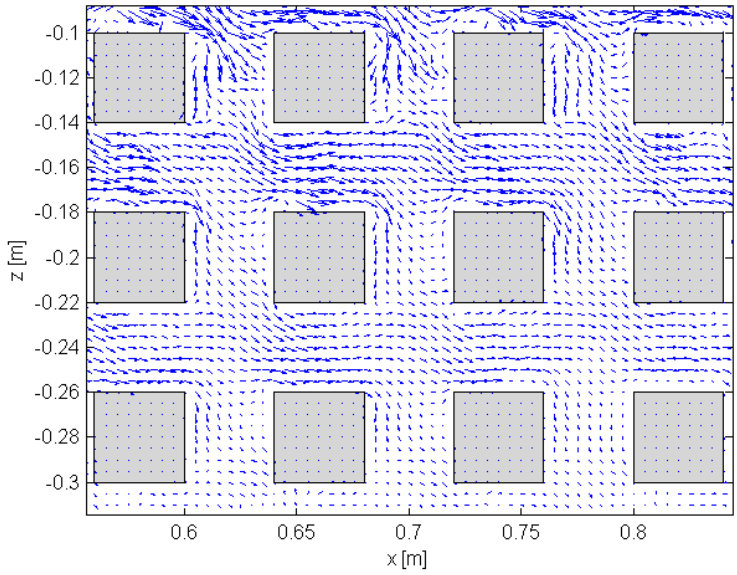

Figure 10: Measured interstitial velocity field.

5 AVERAGED QUANTITIES

The measured velocities inside each pore were averaged over the area of the pore to yield a spatial averaged quantity that is often used to describe flow inside porous domains. The spatially averaged velocity field is shown in Figure 11 (top). The spatial averaged velocity field was further averaged over time for the duration of one wave period to yield a time and spatial averaged vector field. The time averaged vector field is shown in Figure 11 (bottom).

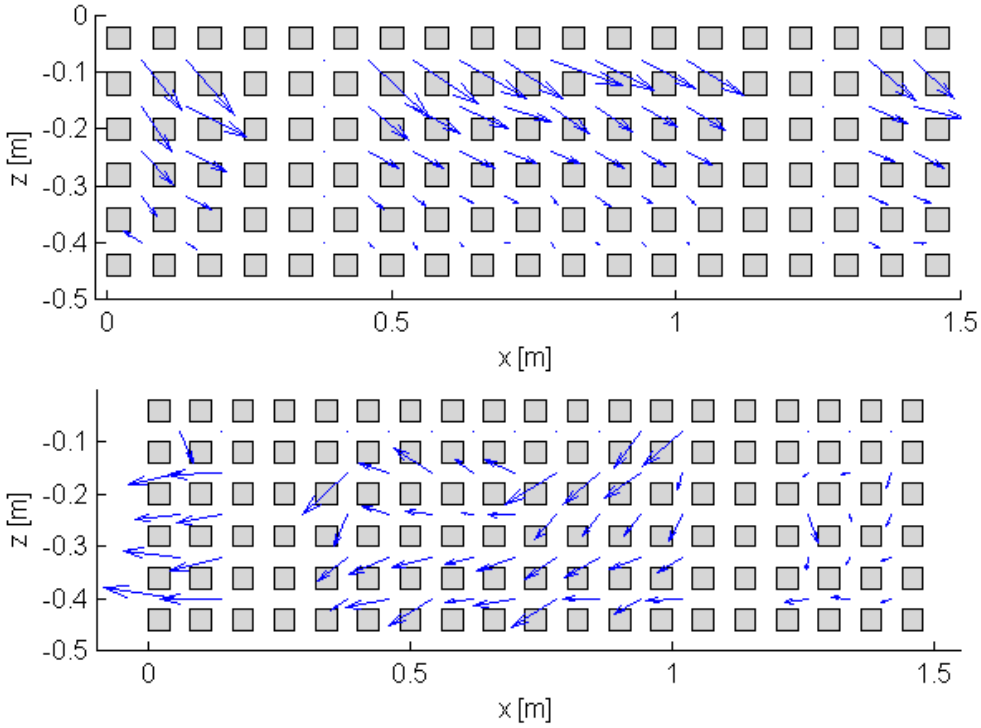

Figure 11: Spatially averaged velocity field at an instant in time (t = 0.4 s) (top) and time averaged over one wave period (bottom)

The time averaged vector field shows the wave induced return current going towards the incident wave, which is from the left. The magnitude increases with the change in wave height. Losada *et al.*, 1998, formulated a theory on mean wave induced flows inside a porous medium. They have also performed quantitative experiments with a rectangular rubble mound breakwater that support the theory. According to the authors' knowledge there have been no detailed measurements of the return current inside a porous medium.

6 CONCLUSIONS

A two-dimensional, rectangular porous structure was built from timber beams and arranged in a non-staggered array. Regular waves with a period of 1 second were generated in a glass flume with the structure in place. The wave reflection and transmission in the structure was observed.

The portion of the array that was below the waterline was divided into 70 overlapping regions. The regions were seeded with neutrally buoyant microspheres and photographed with a high speed camera at 100 frames per second. The water levels inside the porous structure were simultaneously measured with capacitance probes.

The velocity field in each pore was calculated with PIV techniques. All pore velocity fields were then synchronised in time and merged to form a single velocity field for the porous domain.

Spatial averaging was performed on the velocity data to describe the mean properties of the transmitted wave. Further time averaging was used to determine the mean wave induced flows inside the porous medium.

ACKNOWLEDGEMENT

I would like to thank:

1. Prof. Smit from Stellenbosch University, South Africa, for the financial support to acquire the materials used in the experiments.
2. The Mechanical Engineering department of Stellenbosch University, South Africa, for the use of their high speed camera.
3. The CSIR Coastal Hydraulic Laboratory in Stellenbosch, South Africa, for the use of their glass flume and making support personal available.
4. Hannes Zietsman from CSIR DPSS for the custom made light source.

REFERENCES

D'Errico, J., 2012. inpaint_nans (https://www.mathworks.com/matlabcentral/fileexchange/4551), *MATLAB Central File Exchange.*

Higuera, P., Lara, J.L. and Losada, I.J., 2014. Three-dimensional interaction of waves and porous coastal structures using OpenFOAM®. Part I: Formulation and validation. *Coastal Engineering*, *83*, pp.243-258.

Kondo, H. and Toma, S., 1973. Reflection and transmission for a porous structure. In *Coastal Engineering 1972* (pp. 1847-1866).

Losada, I.J., Dalrymple, R.A. and Losada, M.A., 1998. Wave-induced mean flows in vertical rubble mound structures. *Coastal engineering*, *35*(4), pp.251-281.

Losada, I.J., Losada, M.A. and Martin, F.L., 1995. Experimental study of wave-induced flow in a porous structure. *Coastal Engineering*, *26*(1-2), pp.77-98.

Ma, G., Shi, F., Hsiao, S.C. and Wu, Y.T., 2014. Non-hydrostatic modeling of wave interactions with porous structures. *Coastal Engineering*, *91*, pp.84-98.

Madsen, O.S., 1974. Wave transmission through porous structures. *Journal of the Waterways, Harbors and Coastal Engineering Division*, *100*(3), pp.169-188.

Madsen, O.S. and White, S.M., 1976. *Reflection and Transmission Characteristics of Porous Rubble-Mound Breakwaters*. MASSACHUSETTS INST OF TECH CAMBRIDGE DEPT OF CIVIL ENGINEERING.

Madsen, P.A., 1983. Wave reflection from a vertical permeable wave absorber. *Coastal Engineering*, *7*(4), pp.381-396.

Mansard, E.P. and Funke, E.R., 1980. The measurement of incident and reflected spectra using a least squares method. In *Coastal Engineering 1980* (pp. 154-172).

Mellink, B.A., 2012. *Numerical and experimental research of wave interaction with a porous breakwater*. MSc thesis Delft University of Technology, Delft, The Netherlands.

Raffel, M., Willert, C.E. and Kompenhans, J., 2007. *Particle image velocimetry: a practical guide*. Springer Science & Business Media.

Sollitt, C.K. and Cross, R.H., 1976. Wave reflection and transmission at permeable breakwaters. *US Army Corps of Engineers, Coastal Engineering Research Centre*, Tech. Paper 76-8, 172 pp.

Thielicke, W. and Stamhuis, E., 2014. PIVlab–towards user-friendly, affordable and accurate digital particle image velocimetry in MATLAB. *Journal of Open Research Software*, *2*(1).

Westerweel, J. and Scarano, F., 2005. Universal outlier detection for PIV data. *Experiments in fluids*, *39*(6), pp.1096-1100.